Fifth Mississippi State Conference on Differential Equations and Computational Simulations, *Electronic Journal of Differential Equations*, Conference 10, 2003, pp. 55–69.
ISSN: 1072-6691. URL: http://ejde.math.swt.edu or http://ejde.math.unt.edu
ftp ejde.math.swt.edu (login: ftp)

TIN MELTING: EFFECT OF GRID SIZE AND SCHEME ON THE NUMERICAL SOLUTION

VASILIOS ALEXIADES, NOUREDDINE HANNOUN, & TSUN ZEE MAI

Abstract. Benchmark solutions in Computational Fluid Dynamics are necessary for testing and for the verification of newly developed algorithms and codes. For flows involving heat transfer coupled to solid-liquid phase change and convection in the melt, such benchmark solutions do not exist. A set of benchmark problems has recently been proposed for melting of metals and waxes and several researchers responded by providing solutions for the given problems. It was shown in two recent publications that there were large discrepancies in the results obtained by those contributors. In the present, work we focus on one of the four test problems, tin melting at Rayleigh number $Ra = 2.5 \times 10^5$. Solutions obtained for several grids and two discretization schemes are presented and compared. Our results are used to explain the origin of the discrepancies in earlier results. Suggestions for future work are also provided.

1. Introduction

Problems of *melting* frequently arise in natural and industrial processes [1]. Applications include river, lake, and polar melting, magma dynamics, thermal energy storage, casting and molding, crystal growth, welding, coating, and vapor spray deposition, laser processing, thawing of frozen food, preserved organs, tissue cultures, and many more.

Mathematical models describing such *phase change problems* are not amenable to standard analytical tools when flow in the melt is involved. The problems are (de facto nonlinear) *moving boundary problems*. For this reason, the research community has been actively working, mostly during the last two decades, on the development of numerical techniques suitable for phase-change problems. This was motivated by the increasing availability of highly powerful computers along with efficient software.

Numerical methods dealing with phase change problems may be classified into three main categories. The first includes *front tracking methods* [9, 5, 33, 18, 12, 26] that consider the solid-liquid interface as a boundary between two domains (solid and liquid) where distinct sets of conservation equations are solved. An additional

1991 *Mathematics Subject Classification.* 80A22, 74S10, 76D05, 65N99.
Key words and phrases. Phase change, melting, numerical simulation, enthalpy method, benchmark, fluid flow.

Published February 28, 2003.

boundary condition is specified at the interface to account for heat transfer between the two domains. These methods require a moving adaptive grid that distorts as time proceeds to mimic both shape and position of the interface. Therefore, they are not suitable for problems involving highly distorted interfaces or mergers and breakups. The second category of numerical method includes the so called *fixed grid techniques* [29, 30, 4, 31, 32, 16, 24, 26] for which a single set of equations is used for the entire computational domain (solid + liquid). Transfer of latent heat and extinction of velocities in the solid are accounted for through the inclusion of appropriate source terms in the transport equations. In addition to using a simpler model, fixed grid techniques (commonly known as *enthalpy methods*) offer the highly acknowledged benefit of the possibility of using a fixed Cartesian grid for the entire calculations. A third category of numerical methods known as *Eulerian-Lagrangian methods* [15, 27] attempts to combine features of the other two methods.

The problem of "*Gallium melting in a rectangular enclosure heated from the side*" has been one of the most popular problems for assessing the validity of newly developed techniques for phase change coupled to convection in the liquid. This problem has received considerable interest from both experimentalists [11, 6, 7] and CFD (computational fluid dynamics) practitioners [4, 8, 28, 14, 18, 24, 22, 23]. However, all comparisons were mostly qualitative, exhibiting rather large discrepancies among numerical methods and experimental results [4, 18]. The controversial work of Dantzig [8], and later the illuminating work of Stella and Giangi [23], have cast a doubt on the validity of past numerical simulations. Both authors have found flow patterns with several rolls in contrast to other publications where only a single roll was observed. However, this seems to be contradicted by experimental observations.

As a result of the lack of a reference solution (*benchmark solution*) for phase change problems, Gobin and Lequere [17] have promoted a comparison exercise with the purpose of obtaining reference solutions that could be used by code developers to *verify* [21] their own code. In that exercise, four test problems were suggested, two for paraffin waxes (high Prandtl number Pr), and two for metals (low Pr). The first set of results has been presented in two publications [2, 10], the emphasis being mostly on a qualitative comparison. The authors concluded that there were still too large discrepancies between the results from various participants and argued it would be necessary to perform additional simulations. They suggested that participants perform grid refinement studies and validate their own codes on simpler configurations. The most striking results were the fact that the less accurate numerical solutions were actually those which best agreed with experiments.

In this paper, we focus on one of the four test problems of the comparison exercise [2, 10], Case 2 for tin melting at Rayleigh number $Ra = 2.5 \times 10^5$. We present results obtained with the same code for two discretization schemes. We want to provide an answer to whether or not the solution presented by most contributors to the Benchmark exercise were converged or not. We conclude the study by a discussion about the possible origin of the discrepancies between numerical results and experiments as well as between results of the contributors to the comparison exercise.

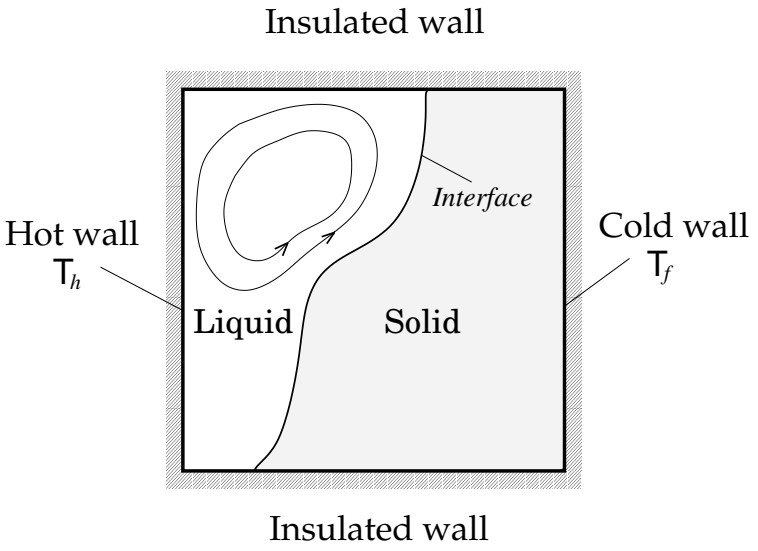

FIGURE 1. Configuration under study : melting of tin in a square cavity

2. Physical problem

The configuration under study is well documented in [2, 10]. A sketch of the problem is shown in Figure 1. A square cavity (width $W = H$ height) filled with tin (pure metal) is initially at freezing temperature $T = T_f$ (tin is solid). The top and bottom boundaries are adiabatic (thermally insulated), while the right boundary is maintained at constant temperature T_f. At time $t = 0$, the left boundary is suddenly brought to a hot temperature T_h larger than the melting temperature. Heat transfer by conduction results in the melting of tin in the cavity. Thermal gradients generate density gradients which in turn drive convection in the liquid tin. Hence, the solid-liquid interface is no longer planar (as for the pure conduction regime). We are interested in the motion as well as the shape of the solid-liquid interface as melting proceeds. The study will also focus on the flow pattern in the liquid as well as the heat transfer process.

3. Mathematical model – Governing equations

The numerical simulations are carried out based on the transport equations (1a–d) which were developed in [4].

Mass

$$\frac{\partial \rho}{\partial t} + \nabla \cdot (\rho \vec{V}) = 0 \tag{1a}$$

Momentum

$$\frac{\partial \rho u}{\partial t} + \nabla \cdot (\rho \vec{V} u) = \nabla \cdot (\mu \nabla u) - \frac{\partial P}{\partial x} - Au \tag{1b}$$

$$\frac{\partial \rho v}{\partial t} + \nabla \cdot (\rho \vec{V} v) = \nabla \cdot (\mu \nabla v) - \frac{\partial P}{\partial y} - Av + \rho_{\text{ref}} g \beta (h - h_{\text{ref}})/c_p \tag{1c}$$

Energy

$$\frac{\partial \rho h}{\partial t} + \nabla \cdot (\rho \vec{V} h) = \nabla \cdot (\alpha \nabla h) - \frac{\partial \rho \Delta H}{\partial t} - \nabla \cdot (\rho \vec{V} \Delta H) \tag{1d}$$

In these equations, ρ stands for density, T for temperature, P for pressure, $\vec{V}$ for velocity vector, u and v for x and y components of velocity, h for sensible enthalpy, ΔH for latent enthalpy content, μ for dynamic viscosity, λ for thermal conductivity, c_p for specific heat, α for λ/c_p, β for coefficient of thermal expansion, g for gravitational acceleration, t for time and x and y for Cartesian coordinates. The subscript "ref" is used for reference quantities.

The flow is assumed to two dimensional, unsteady, and obeys the Navier-Stokes equations for incompressible Newtonian fluids written in Cartesian coordinates (eq. 1a-c). The thermophysical properties (c_p, λ, α, μ, β) are independent of temperature and are the same for both solid and liquid. The model also assumes that density ρ may vary with temperature. However the present simulations assume a constant density along with the Boussinesq approximation (density variations due to temperature gradients are accounted for in buoyancy terms).

The present formulation is a one-domain method wherein the same set of equations is used for both solid and liquid. The material in the cavity is regarded as a porous medium with porosity varying with liquid fraction through Carman-Kozenay's law. The constant A in the source term of the momentum Equations (1b, 1c) has the form:

$$A = -\frac{C(1-f_L)^2}{f_L^3 + q} \tag{2}$$

where f_L is the liquid fraction and C and q are two constants chosen to ensure driving the velocities to zero in the solid, while maintaining a convergent algorithm. The source term S_h:

$$S_h = -\frac{\partial \rho \Delta H}{\partial t} - \nabla \cdot (\rho \vec{V} \Delta H) \tag{3}$$

in the right hand side of the energy equation (1d) accounts for latent enthalpy transfer during phase change.

4. Numerical method

A finite volume method is used to discretize Equations (1a–d) on a Cartesian uniform grid with staggered arrangement for the velocities [13]. Each equation is integrated on a control volume centered at a node of the main variable for that equation. Second order accuracy is retained for quadratures, source terms and diffusion terms. Convective fluxes are approximated with the formalism of Patankar [19] which allows one to choose among five different schemes (upwind, hybrid, centered, exponential, and power law). Time discretization is fully implicit (Euler Backward). Nonlinearity and coupling between the various equations is handled by the SIMPLER algorithm of Patankar [20].

The energy equation requires a special treatment due to the presence of latent enthalpy content in the source terms arising from phase change. To obtain the new enthalpy value h^{k+1} for the current outer iteration $(k+1)$, one needs ΔH^{k+1} which itself depends on the unknown solution h^{k+1}. The process for handling this problem is described in [4]. At each outer iteration $(k+1)$ the latent enthalpy

content is updated from the values at the previous outer iteration (k) through the formula:

$$\Delta H^{k+1} = \Delta H^k + \omega_{\Delta H} \frac{a_P^h}{a_P^{oh}} \left\{ h^k - c_p \left[\frac{T_L - T_S}{L} \Delta H^k + T_S \right] \right\} \tag{4}$$

In equation (4), a_P^h and a_P^{oh} stand for the central coefficient of the discretized energy equation and the unsteady term coefficient respectively [4], while $\omega_{\Delta H}$ is a relaxation factor used to avoid divergence of outer iterations. Latent enthalpy content ΔH is related to temperature T through a linear relationship over a small interval $\epsilon = T_L - T_S$ where T_L and T_S are the liquidus and solidus temperatures respectively. for $T > T_L$ the latent enthalpy content is equal to the latent heat, L while for $T < T_S$ it is zero.

After relation (4) is applied at every node of the computational domain, an overshoot cutoff procedure (5) is used to ensure that ΔH lies between 0 and L.

$$\Delta H^{k+1} = \begin{cases} L & \text{if} \quad \Delta H^{k+1} \geq L \\ 0 & \text{if} \quad \Delta H^{k+1} \leq 0 \end{cases} \tag{5}$$

The new enthalpy h^{k+1} may then be obtained from the energy equation (1d) using the known values of ΔH^{k+1}.

To ensure a better consistency between temperature T and liquid fraction f_L obtained at a given outer iteration, several sweeps are performed over equations (1d,4). This amounts to performing an energy update loop within the outer iteration.

The linear systems obtained at each step of the numerical procedure are solved with two solvers. A BICGSTAB-SIP solver is used for each of u, v, h and pressure equations while the pressure correction and streamfunction equations are solved with a CG-SSIP solver. The latter equation is needed to recover the streamlines from the velocity field for plotting purposes.

5. Numerical parameters and experiments

It is a standard practice to pick the numerical range of solidification $[T_S, T_L]$ centered at the physical freezing temperature T_f. For our application, the coldest boundary temperature is prescribed and equal to T_f. The Maximum Principle implies that nowhere and at no time should the temperature be smaller than the melting temperature. This led us to pick the choice: $T_S = T_f$ and $T_L = T_f + \epsilon$.

Table 1 gives the physical parameter values used for the numerical simulations. These correspond to Case#2 of the Benchmark problems [2]. Simulations are carried out up to time $1000s$ for three grids (100×100, 200×200, and 400×400) and two discretization schemes (upwind and hybrid).

Inner iterations are stopped when the 1–norm of the residual is reduced by a factor ϵ_i set to 10^{-7} for the u, v, h, and pressure equations, and to 10^{-5} for the pressure correction equation. In addition, an upper bound is preset for the total number of inner iterations. This upper bound is grid as well as time dependent for the pressure correction equation, while a value of 10 works fine for the other four equations and for all computations.

The convergence criterion for outer iterations is based on a total number of outer iterations rather than a prescribed value for the residual. The choice of total number of outer iterations is based on the monitoring of the outer iteration errors (ratio of the norms of the difference between two consecutive iterates $\mid \phi^{k+1} - \phi^k \mid$ and the difference between the first two iterates, where ϕ stands for any of u, v,

Tin properties		
Thermal conductivity	λ	60 (W/m K)
Specific heat	c_p	200 (J/Kg K)
Coefficient of thermal expansion	β	2.67×10^{-4} (K^{-1})
Kinematic viscosity	ν	8×10^{-7} (m^2/s)
Density	ρ	$7,500$ (Kg/m^3)
Latent heat of fusion	L	6×10^4 (J/Kg)
Fusion temperature	T_f	505 (K)
Other parameters		
Gravity	g	10 (m^2/s)
Cavity size (height, width)	H, W	0.1 (m)
Hot wall temperature	T_h	508 (K)
Dimensionless numbers		
Rayleigh number	$R_a = g\beta(T_h - T_f)H^3/\alpha\nu$	2.5×10^5
Prandtl number	$P_r = \nu/\alpha$	0.02
Stefan number	$St = c_p(T_h - T_f)/L$	0.01

TABLE 1. Physical parameter values

h, or P). The total number of outer iteration is determined by trial and error. The number selected is one after which the outer iteration error was not decreasing anymore. The residuals are checked as well to ensure that an appropriate level is reached. The values for total number of outer iterations and energy sweeps retained for the various runs are as follows: 60 and 5 for coarse grids (100×100), 80 and 1 for fine grids (200×200), and 80 and 6 for very fine grids (400×400).

The time steps used for the calculations vary from $\Delta t = 1s$ down to $0.1s$. The solidification range is set to $\epsilon = 0.025$ and the constants in the momentum source terms take on the values $C = 10^{15}$ and $q = 10^{-6}$. Under-relaxation factors are used for outer iterations: $\omega_u = 0.7$, $\omega_h = 0.8$, $\omega_P = 0.9$, $\omega_{\Delta H} = 0.3$ where subscripts refer to the corresponding equation's main variable.

6. RESULTS

Streamlines. Figures 2 and 3 display the streamlines in the melt as well as the solid-liquid interface obtained by the upwind and hybrid schemes respectively. The plots are given at four times, ranging between $250s$ and $1000s$ and for three grid sizes (100×100, 200×200, and 400×400). The solid-liquid interface is where liquid fraction contour value $f_L = 0.5$. Only part of the computational domain is displayed: the left boundary of each figure corresponds to the hot wall, while the solid area to the right of the interface has been truncated. At time $250s$, the upwind scheme (Fig.2) shows one, two, and three rolls for the 100×100, 200×200, and 400×400 grids respectively. A similar scenario may be observed for the hybrid scheme (Fig.3) at time $400s$. As expected, the hybrid scheme is overall more accurate than the upwind scheme. For example, at time $250s$ with a 100×100 grid,

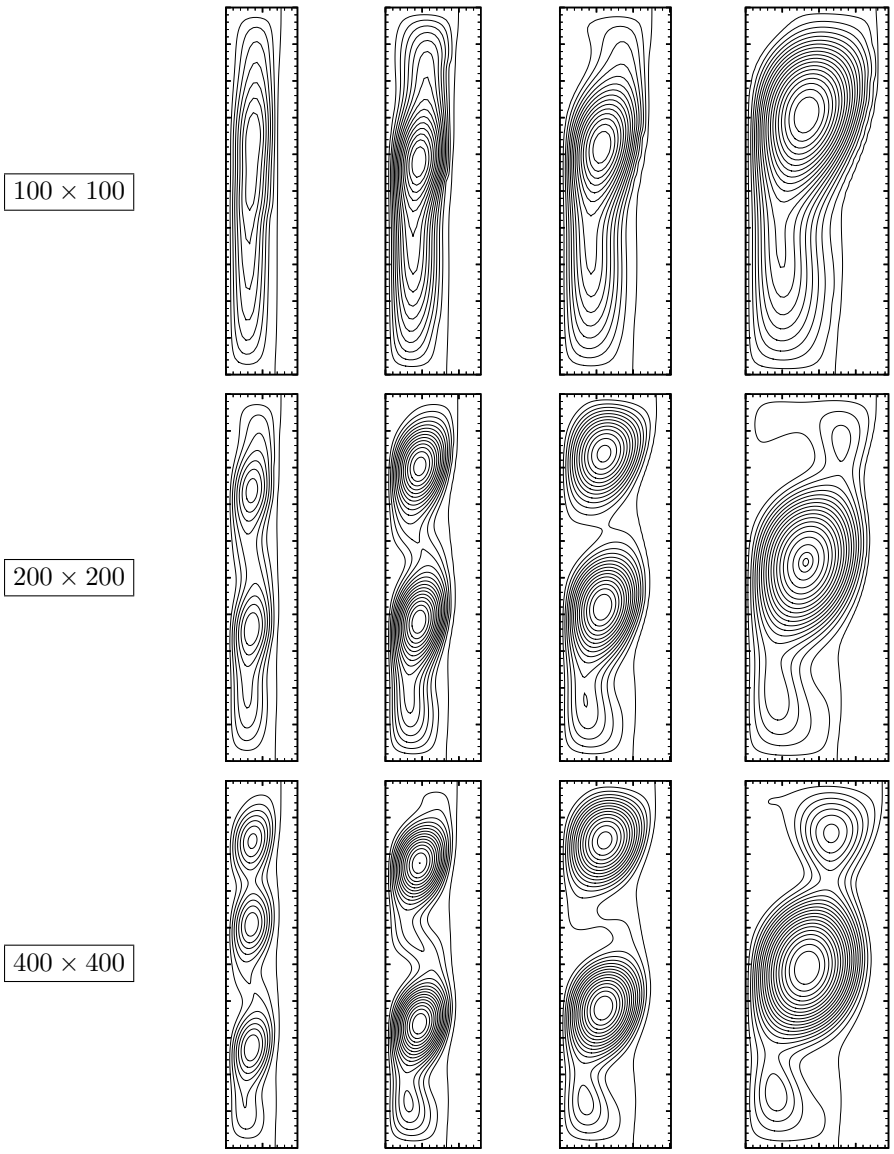

FIGURE 2. Upwind scheme : streamlines and solid-liquid interface at several times for three choices of grid

only one roll is obtained with the upwind scheme while two are gotten with the hybrid scheme. Similarly, for a 200×200 grid, two rolls are obtained with the upwind scheme and three with the hybrid scheme. At the same time 250s and for the finer grid 400×400, both upwind and hybrid scheme show three rolls but those for hybrid scheme are stronger than the ones for upwind scheme.

At later times, a smaller number of rolls remain in the cavity, due to the merging of the original rolls. Finer grids 400×400 capture two rolls at time $1000s$ even with the upwind scheme. But this shows that a very fine grid is necessary in order to get the accuracy desired. That could explain why most of the Benchmark contributors [2, 10] did not get a two roll structure at that time since they used grids coarser than 100×100.

Interface. The number of rolls present in the liquid has a strong influence on both the shape and position of the solid-liquid interface. This may be observed on the interface plots shown in Figure 4 for both upwind and hybrid schemes. The plots show the solid-liquid interface at several times and for three grid sizes (100×100, 200×200, and 400×400). The interface moves from left to right as time increases. At time $100s$, the interface is identical for all three grids (and both schemes). Moreover the interface is flat as for the pure conduction regime. This is due to the fact that only one roll is present in the cavity and the convection is not strong enough to affect the interface shape. At time $250s$ the interface acquires a wavy shape due to faster melting at the rolls locations (3 bumps for hybrid scheme and 400×400 grid corresponding to 3 rolls in the liquid). As time proceeds, the depth of the bumps increases and the difference between fine grid and coarse grid solutions becomes more pronounced. The benchmark contributors [2, 10] were divided into two groups. In the first group, the largest, contributors found a one bump interface at time $1000s$, while in the second group, a two-bump interface was reported. Clearly, our results indicate that finer grids will result in more bumps on the interface for both the upwind and the hybrid scheme. Another interesting fact to notice is that the interface position at the bottom wall seems to be insensitive to the accuracy of the solution elsewhere (number of rolls captured). therefore, this parameter should not be retained as a criterion for evaluating the accuracy of the solution. On the other hand, the top part of the interface is strongly affected by the number of rolls present in the cavity.

Number of rolls. Figure 5 summarizes the flow patterns obtained by both upwind and hybrid scheme for three grid sizes (100×100, 200×200, and 400×400). The number of rolls present in the cavity at a given time is indicated by a corresponding number of small circles (3 circles→3 rolls). Each jump or drop of the solid horizontal line, for a particular choice of scheme and grid size, corresponds to a merging of two rolls into one. Consequently, the total number of rolls is reduced by one.

The sketch shows that at early times only one roll is present in the cavity. Later, as many as four rolls are captured for some choices of scheme and grid size. The number of rolls decreases afterward from four to three, then two, and one, as time proceeds. It may be noticed that the number of rolls present in the cavity at any particular time is larger for finer grids and higher order schemes.

Nusselt number. Another parameter monitored by the benchmark contributors [2, 10] is the average Nusselt number at the hot wall defined by Equation 6.

$$Nu = \int \lambda \left.\frac{\partial T}{\partial x}\right|_w dy \Big/ \lambda \frac{(T_f - T_h)}{W} H \tag{6}$$

Figure 6 displays the time evolution of Nu for the upwind scheme (left) and hybrid scheme (right), and for three choices of grid. The correlation proposed by the benchmark contributors [2] is also represented in each subfigure.

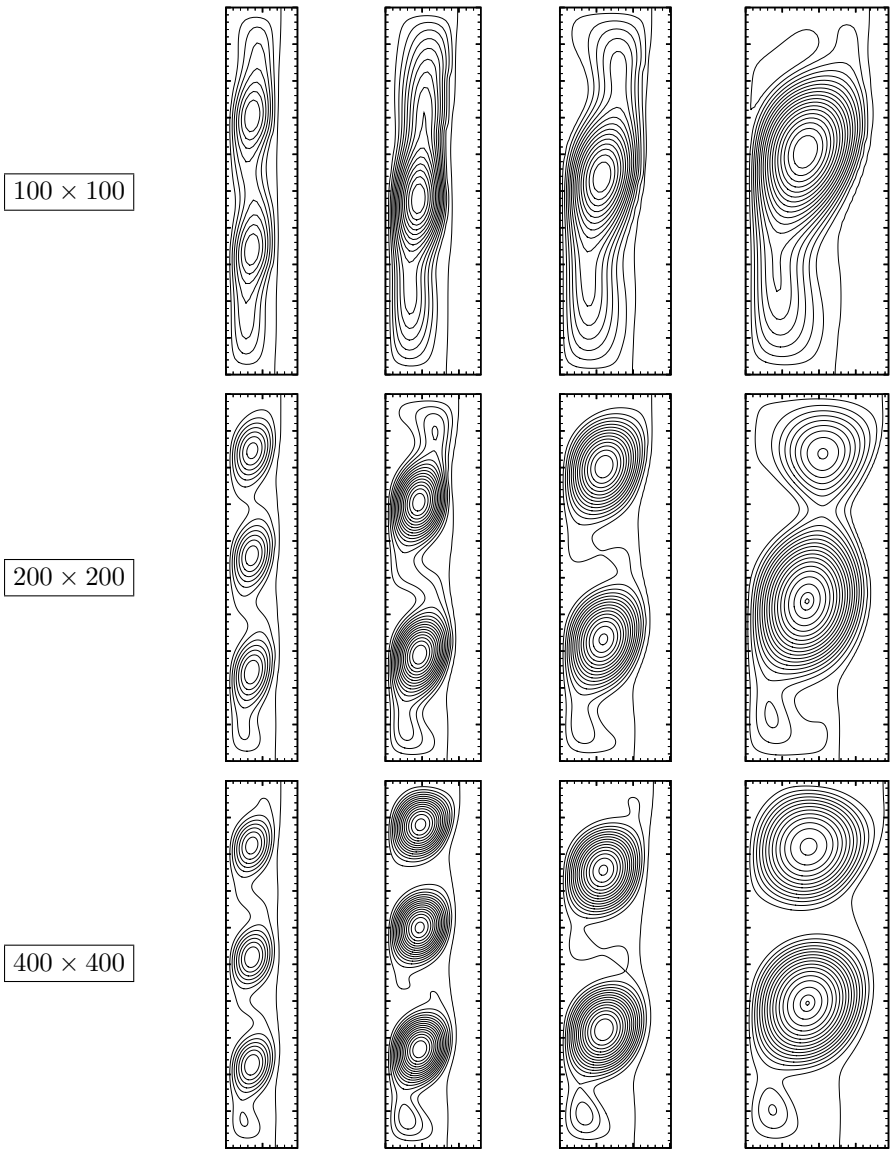

FIGURE 3. Hybrid scheme : streamlines and solid-liquid interface at several times for three choices of grid

As may be seen on the plots, coarse grid (100×100) curves agree very well with the correlation. The step like pattern at early times on the Nu curves is due to the use of an enthalpy method with too coarse a grid. On the other hand, finer grid solutions return higher values of the Nusselt number and the plots exhibit sudden drops corresponding to roll merging. The larger values of the Nusselt number for

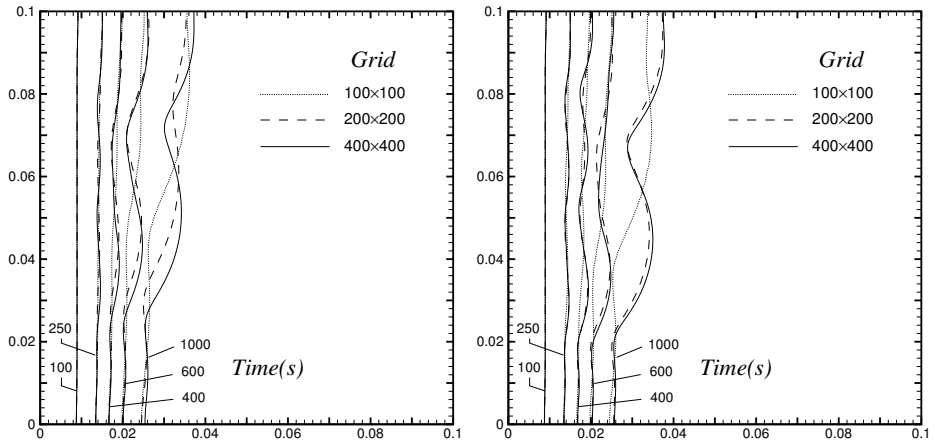

(a) Upwind scheme (b) Hybrid scheme

FIGURE 4. Solid-liquid interface at times 100, 250, 400, 600, 1000s for three grid sizes and two discretization schemes

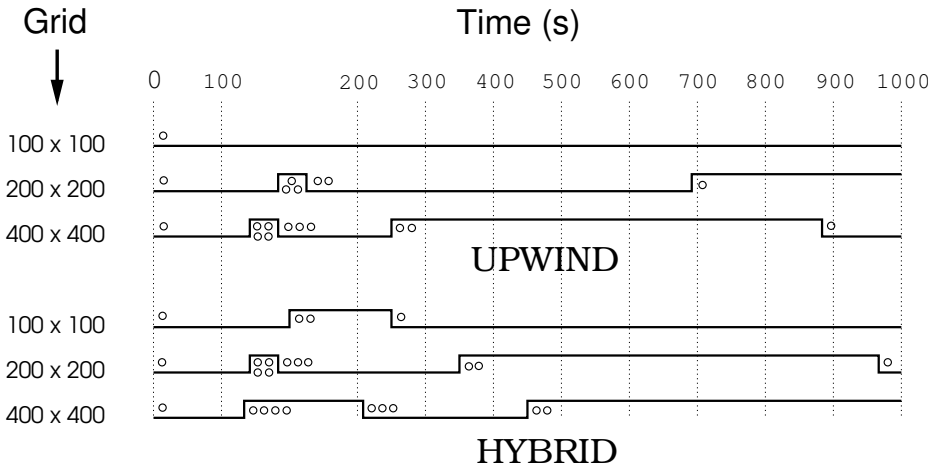

FIGURE 5. Number of rolls as a function of time for two discretization schemes (upwind top and hybrid bottom) and three choices of grids

finer grids may be explained by the stronger convection in the liquid, resulting in higher heat transfer near the wall.

Volume of melt. The total fraction of liquid in the cavity as a function of time is displayed in Figure 7. The volume of melt achieved is seen to increase with the number of rolls present in the cavity (finer grids and higher order discretization schemes). Therefore, more accurate solutions are expected to return faster melting

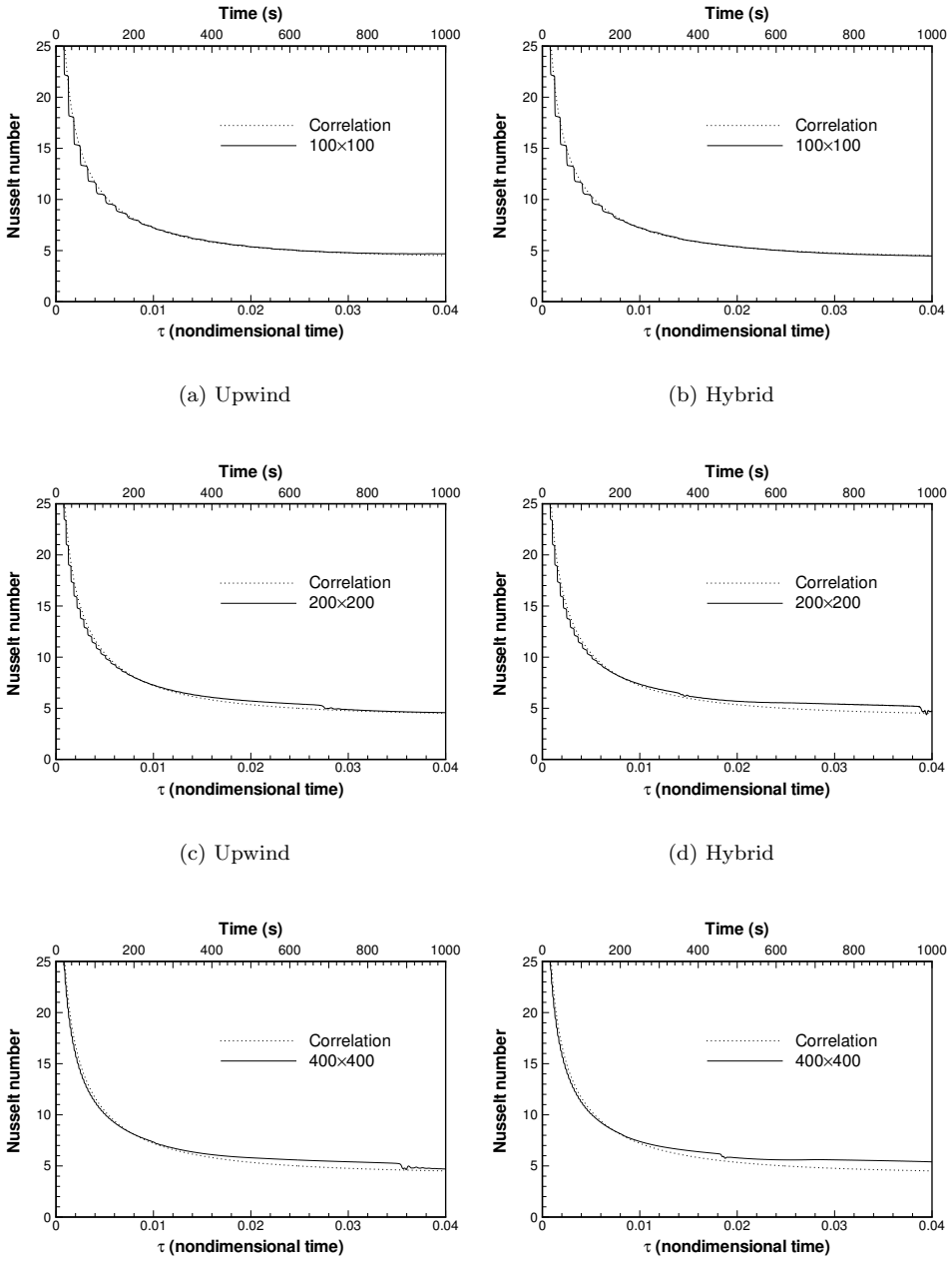

(a) Upwind (b) Hybrid

(c) Upwind (d) Hybrid

(e) Upwind (f) Hybrid

FIGURE 6. Time evolution of the average Nusselt number at the hot wall. Left figures (a, c, e) for upwind scheme and right (b, d, f) figures for hybrid scheme.

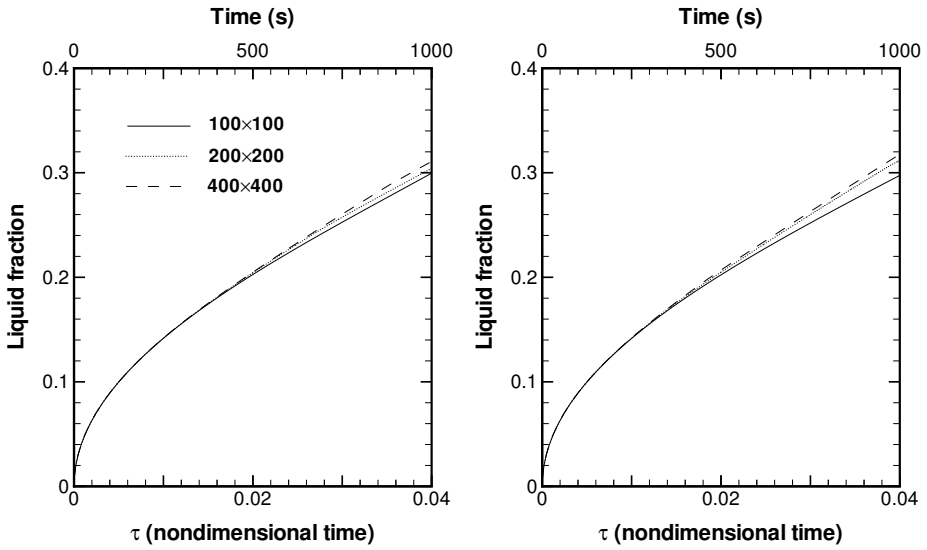

(a) Upwind scheme

(b) Hybrid scheme

FIGURE 7. Time evolution of the total fraction of melt in the cavity for three choices of grid and two discretization schemes

rates. This is a natural expectation since convection is better resolved (stronger) in the liquid.

CPU requirements. Several machines have been used to perform the computations. A run with a 100×100 grid takes about 15 hours on a Sun Ultra 30 workstation. A 200×200 run takes about 60 hours on a CRAY SV1 supercomputer, while a 400×400 run requires about 240 hours on one processor of a Compaq Alphaserver SC clusters. These timings are for the Upwind scheme. Runs with the Hybrid scheme require slightly larger times.

7. Conclusion

In the present work we have performed numerical simulations of a tin melting benchmark problem suggested in [2, 10]. The calculations were done for two choices of discretization scheme (upwind and hybrid) and three grid sizes (100×100, 200×200, and 400×400). Plots were presented for streamlines in the liquid, solid-liquid interface, average Nusselt number at the hot wall, and volume of melt in the cavity.

Our results indicate that more rolls are expected in the liquid as grid is refined and discretization scheme order is increased. In particular, a 100×100 grid is not enough to capture the multiple cell structure of the flow with either the upwind or the hybrid scheme. The roll structure was shown to have a strong impact on the solid-liquid interface shape and position. Therefore a judicious choice of grid and discretization scheme is necessary in order to simulate the flow correctly.

Most contributors to the benchmark exercise [2, 10] used a grid coarser than 100×100 along with either the upwind (mostly) or the hybrid discretization scheme.

Our work indicates that these solutions may not have been sufficiently resolved spatially. This resulted in a solid-liquid interface with a single bump at time $1000s$ in contrast to the two-bump interface shape obtained by four of the benchmark participants as well as in our work.

"*Why do coarse grid solutions agree better with experimental results than fine grid solutions?*" is a question that still needs to be addressed. This issue was actually raised for the problem of Gallium melting [11], since to date, there are no experimental results for the melting of tin. We suggest two possible ideas. First, the experimental setup may not have reproduced exactly the model assumptions. The two-dimensional assumption generally requires a long cavity in the transverse direction, uniform initial temperature and isothermal boundaries are generally difficult to implement experimentally, and the visualization is particularly difficult due to the opacity of the melt. A second path to follow in order to explain the discrepancies between experiments and numerical results is the validity of the mathematical model and in particular the basic assumptions such as two-dimensionality, no expansion upon melting, and constant thermophysical properties. This work has shown that the solution of the mathematical model used for simulating the benchmark problem is expected to be a multiple-roll solution.

The current work is in progress. Results for higher order schemes and longer melting times will be presented soon and a summary of all the results obtained will be compiled.

Acknowledgment. The authors want to thank Dr D. Gobin for having graciously communicated some of the benchmark results.

Access to the Compaq AlphaServer SC computer was provided by the Center for Computational Sciences at Oak Ridge National Laboratory and the Evaluation of Early Systems research project, sponsored by the Office of Mathematical, Information, and Computational Sciences, Office of Science, U.S. Department of Energy under Contract No. DE-AC05-00OR22725 with UT-Battelle, LLC. The U.S. Government retains a non-exclusive, royalty-free license to publish or reproduce the published form of this contribution, or allow others to do so, for U.S. Government purposes. Oak Ridge National Laboratory is managed by UT-Battelle, LLC for the United States Department of Energy under Contract No. DE-AC05-00OR22725.

Access to the Cray SV1 supercomputer was provided by the Alabama Supercomputer Authority which provides supercomputing time free of charge to faculty and students of the state funded schools of Alabama.

References

[1] Alexiades, V., Solomon, A. D. *Mathematical modeling of melting and freezing processes.* Hemisphere Publi. Co., Washington DC, 1993.

[2] Bertrand, O., Binet, B., Combeau, H., Couturier, S., Delannoy, Y., Gobin, D., Lacroix, M., Lequere, P., Medale, M., Mencinger, J., Sadat, H., Vieira, G. *Melting driven by natural convection. A comparison exercise: first results.* International Journal of Thermal sciences Vol 38 (1999) pp5-26.

[3] Bonacina, C., Comini, G., Fasans, A., Primiceris, M. *Numerical solution of phase change problems.* International Journal of Heat and Mass Transfer Vol 16 (1973) pp1825-1832.

[4] Brent, A. D., Voller, V. R. and Reid, K. J. *Enthalpy-Porosity technique for modeling convection-diffusion phase change: Application to the melting of a pure metal.* Numerical Heat Transfer Vol 13 (1988) pp 297-318.

[5] Crank, J. *Free and moving boundary problems.* Oxford, Science Publication, NewYork 1984.

[6] Campbell, T. A., Koster, J. N. *Visualization of liquid-solid interface morphologies in gallium subject to natural convection.* Journal of Crystal Growth Vol 140 (1994) pp414-425.

[7] Campbell, T. A., Pool, R. E., Koster, J. N. *Melting and solidification of a liquid metal at a vertical wall.* AIAA-94-0792.

[8] Dantzig, J. A. *Modeling liquid-solid phase changes with melt convection.* International Journal for Numerical Methods in Engineering Vol 28 (1989) pp1769-1785.

[9] Ettouney, H. M., Brown, R. A. *Finite-element method for steady solidification problems.* Journal of Computational Physics Vol 49 (1983) pp118-150.

[10] Gobin, D., Lequere, P. *Melting from an isothermal vertical wall. Synthesis of a numerical comparison exercise.* Computer Assisted Mechanics and Engineering Sciences Vol 7 (2000) pp289-306.

[11] Gau, C., Viskanta, R. *Melting and solidification of a pure metal from a vertical wall.* Transactions of ASME: Journal of Heat Transfer Vol 108 (1986) pp171-174.

[12] Huang, L. J. , Ayyaswamy, P. S., Cohen, I. M. *Melting and solidification of thin wires: a class of phase-change problems with a mobile interface -I. Analysis.* International Journal of Heat and Mass Transfer Vol 38 (1995) pp1937-1645.

[13] Harlow, F. H., Welsh J. E. *Numerical calculation of time-dependent viscous incompressible flow of fluid with free surface.* Physics of Fluids Vol 8 (1965) pp 2182-2189.

[14] Ho, C. J., Chu, C. H. *The melting process of ice from a vertical wall with time-periodic temperature perturbation inside a rectangular enclosure.* International Journal of Heat and Mass Transfer Vol 36 No13 (1993) pp3171-3186.

[15] Juric, D. , Tryggvason, G. *A front tracking method for dendritic solidification.* Journal of Computational Physics Vol 123 (1996) p127.

[16] Kim, J., Lim, I., Yang, H. and Meyers, C. *Comparison of four different latent heat models during the phase change process.* AFS transactions 127 (1992) pp947-954.

[17] Lequere, P., Gobin, D. *Call for contribution.* Website: m17.limsi.fr/Individu/plq/.

[18] McDaniel D. J., Zabaras, N. *A least-squares front-tracking finite-element method analysis of phase change with natural convection.* International Journal for Numerical Methods in Engineering Vol 37 (1994) pp2755-2777.

[19] Patankar, S. V. *Numerical Heat Transfer and Fluid Flow.* Hemisphere Publishing Corporation, New York 1980.

[20] Patankar, S. V. *Elliptic systems: Finite-difference method I.* In Handbook of Numerical Heat Transfer, John Wiley & Sons 1988.

[21] Roache, P. J. *Verification and Validation in Computational Science and Engineering.* Hermosa Publishers, Albuquerque, N. M. 1998.

[22] Rady, A., Mohanty, A. K. *Natural convection during melting and solidification of pure metals in a cavity.* Numerical Heat Transfer Part A Vol 29 (1996) pp49-63.

[23] Stella, F., Giangi, M. *Melting of a pure metal on a vertical wall: numerical simulation.* Numerical Heat Transfer Part A Vol 138 (2000) pp193-208.

[24] Shyy, Y., Rao, M. M. *Enthalpy based formulation for phase change problems with application to g-jitter.* Microgravity Science and Technology VII / 1 (1994) pp41-49.

[25] Shyy, W., Udaykumar, H. S. , Liang, S.-J. *An interface tracking method applied to morphological evolution during phase change.* International Journal of Heat and Mass Transfer Vol 36 (1993) pp1833-1844.

[26] Shyy, W., Udaykumar, H. S. , Rao, M. M. , Smith, R. W. *Computational fluid dynamics with moving boundaries.* Taylor and Francis 1996.

[27] Udaykumar, H. S., Mittal, R. , Shyy, W. *Computation of solid-liquid phase fronts in the sharp interface limit on fixed grids.* International Journal of Computational Physics Vol 153 (1999) pp535-574.

[28] Viswanath, R., Jaluria, Y. *A comparison of different solution methodologies for melting and solidification problems in enclosures.* Numerical Heat Transfer Part B Vol 24 (1993) pp77-105.

[29] Voller, V. R., Cross, M. and Markatos, N. C. *An enthalpy method for convection-diffusion phase change.* International Journal for Numerical Methods in Engineering.

[30] Voller, V. R., Prakash, C. *A fixed grid numerical modeling methodology for convection-diffusion mushy region phase-change problems.* International Journal of Heat and Mass Transfer Vol 30 No8 (1987) pp1709-1719.

[31] Voller, V. R., Swaminathan C. R. *Fixed grid techniques for phase change problems: A review.* International Journal for Numerical Methods in Engineering Vol 30 (1990) pp875-898.
[32] Voller, V. R., Swaminathan C. R. *General source-based methods for solidification phase change.* Numerical Heat Transfer Part B Vol 19 (1991) pp175-189.
[33] Yeoh, G. H. *Natural convection in a solidifying liquid.* Ph.D. Thesis. The university of New South Wales, 1993.

Vasilios Alexiades
Mathematics Department, University of Tennessee, Knoxville, TN 37996-1300 USA,
and, Oak Ridge National Laboratory, Oak Ridge, TN 37831, USA
E-mail address: alexiades@utk.edu

Noureddine Hannoun
Mathematics Department, University of Tennessee, Knoxville, TN 37996-1300, USA
E-mail address: hannoun@math.utk.edu

Tsun Zee Mai
Mathematics Department, Box 870350, The University of Alabama, Tuscaloosa, AL 35487, USA
E-mail address: tmai@gp.as.ua.edu